HHS Public Access

Author manuscript

Biochem J. Author manuscript; available in PMC 2016 January 14.

Published in final edited form as:

Biochem J. 2015 July 1; 469(1): 33–44. doi:10.1042/BJ20150169.

Structural determinants of human proton-coupled folate transporter oligomerization: role of GXXXG motifs and identification of oligomeric interfaces at transmembrane domains 3 and 6

Mike R. Wilson[*,1], **Sita Kugel**[*,1], **Jenny Huang**[*], **Lucas J. Wilson**[*], **Patrick A. Wloszczynski**[*], **Jun Ye**[†], **Larry H. Matherly**[*,‡,§,1,2], and **Zhanjun Hou**[*,§,1,2]

[*]Department of Oncology, Wayne State University School of Medicine, Detroit, Michigan, 48201 U.S.A

[†]Key Laboratory of Urban Environment and Health, Institute of Urban Environment, Chinese Academy of Sciences, Xiamen, 361021 P.R. China

[‡]Department of Pharmacology, Wayne State University School of Medicine, Detroit, Michigan, 48201 U.S.A

[§]Molecular Therapeutics Program, Barbara Ann Karmanos Cancer Institute, Detroit, Michigan, 48201 U.S.A

Abstract

The human proton-coupled folate transporter (hPCFT) is expressed in solid tumours and is active at pHs characterizing the tumour microenvironment. Recent attention focused on exploiting hPCFT for targeting solid tumours with novel cytotoxic anti-folates. hPCFT has 12 transmembrane domains (TMDs) and forms homo-oligomers with functional significance. The hPCFT primary sequence includes GXXXG motifs in TMD2 ($G^{93}XXXG^{97}$) and TMD4 ($G^{155}XXXG^{159}$). To investigate roles of these motifs in hPCFT function, stability and surface expression, we mutated glycine to leucine to generate single or multiple substitution mutants. Only the G93L and G159L mutants preserved substantial [^{3}H]methotrexate (Mtx) transport when expressed in hPCFT-null (R1-11) HeLa cells. Transport activity of the glycine-to-leucine mutants correlated with surface hPCFT by surface biotinylation and confocal microscopy with ECFP*-tagged hPCFTs, suggesting a role for GXXXG in hPCFT stability and intracellular trafficking. When co-expressed in R1-11 cells, haemagglutinin-tagged glycine-to-leucine mutants and His_{10}-tagged wild-type (WT) hPCFT co-associated on nickel affinity columns, suggesting that the GXXXG motifs are not directly involved in hPCFT oligomerization. This was substantiated by *in situ* FRET experiments with co-expressed ECFP*- and YFP-tagged hPCFT. Molecular modelling of dimeric hPCFT structures showed juxtaposed TMDs 2, 3, 4 and 6 as potential structural

[2]Correspondence may be addressed to either author (houz@karmanos.org or matherly@karmanos.org).
[1]These authors contributed equally.

AUTHOR CONTRIBUTION

For this manuscript, Zhanjun Hou and Larry Matherly equally participated in the research design, data analysis and writing. Mike Wilson and Sita Kugel equally contributed in experimental execution. Jenny Huang, Lucas Wilson and Patrick Wloszczynski also assisted in the execution of the experiments. Jun Ye consulted on structure homology modelling and docking.

interfaces between monomers. hPCFT cysteine insertion mutants in TMD3 (Q136C and L137C) and TMD6 (W213C, L214C, L224C, A227C, F228C, F230C and G231C) were expressed in R1-11 cells and cross-linked with 1,6-hexanediyl *bis*methanethiosulfonate, confirming TMD juxtapositions. Altogether, our results imply that TMDs 3 and 6 provide critical interfaces for formation of hPCFT oligomers, which might be facilitated by the GXXXG motifs in TMD2 and TMD4.

Keywords

anti-folate; cross-linking; folate; oligomerization; proton-coupled folate transporter; transporter

INTRODUCTION

Folates are water-soluble members of the B-class of vitamins. They act as one-carbon carriers in metabolic reactions leading to biosynthesis of purines, thymidylate, methionine, histidine and serine [1]. Because of their hydrophilic character, there is minimal passive diffusion of folates across cell membranes. Rather, highly specific transporters are required to mediate intestinal folate absorption and folate uptake into systemic tissues [2]. Three primary transport routes are involved in folate internalization, including the reduced folate carrier (RFC), the proton-coupled folate transporter (PCFT) and folate receptors α and β. These systems contribute to *in vivo* folate homeostasis and to delivery of cytotoxic anti-folates including methotrexate (Mtx) and pemetrexed (Pmx) in the treatment of cancer [2–4].

PCFT (SLC46A1) is a proton-folate symporter that functions optimally at acidic pH by coupling the flow of protons to the transport of folates [5–7]. The role of PCFT in intestinal folate absorption in humans was established by demonstrating loss-of-function mutations in human PCFT (hPCFT) in a patient with the rare autosomal inherited disorder, hereditary folate malabsorption [7]. In addition to the proximal small intestine, hPCFT is expressed in other normal tissues, such as liver and kidney, which do not experience low pH conditions [4,8]. hPCFT is detected at substantial levels in many human tumours [9,10] and shows appreciable activity at pH 6.5–6.8, depending on the substrate, although maximal activity occurs at pH 5–5.5 and transport is nominal above pH 7 [5,11]. The clinically relevant anti-folate Pmx is among the best substrates for hPCFT and at least part of its clinical efficacy is probably due to its membrane transport by hPCFT [3]. Most recently, novel cytotoxic folate analogues are being developed with transport specificities for PCFT over RFC for selectively targeting solid tumours [3,9, 12–17].

Reflecting its biological and therapeutic importance, studies have begun to explore key structural determinants of hPCFT function [3,18,19]. Thus, structurally and/or functionally important residues in hPCFT were identified, including Asp^{109}, Arg^{113}, Asp^{156}, Gly^{158}, Leu^{161}, Ser^{172}, Glu^{185}, Ile^{188}, Gly^{189}, Gly^{192}, Glu^{232}, His^{247}, His^{281}, Ile^{304}, Arg^{376} and Pro^{425} [3,20–29], and stretches including transmembrane domains (TMDs) 2, 4 and 5 were identified by cysteine-scanning accessibility methods as forming substrate-binding/membrane-translocation domains [20,21,30]. hPCFT is N-glycosylated at Asn^{58} and Asn^{68}

[31]. A unique β-turn structure in the TMD 2–3 loop region forms a novel reentrant loop structure [30] and is essential for intracellular trafficking and high level transport [26,32].

hPCFT forms homo-oligomers both in detergent solution and *in situ* with the hPCFT dimer as the dominant form [18]. With ectopically expressed hPCFT, oligomerization was established by cross-linking with 1,1-methanediyl *bis*methanethiosulfonate (MTS-1-MTS), blue native gel electrophoresis, binding of co-expressed haemagglutinin (HA) and His_{10}-tagged hPCFT monomers to nickel affinity columns and FRET between co-expressed YFP (YPet)- and enhanced cyan fluorescent protein (with K26R/N164H mutation; ECFP*)-tagged hPCFT monomers [18]. Combined wild-type (WT) and inactive mutant P425R hPCFTs exhibited a distinctive 'dominant-positive' transport phenotype, implying positive co-operativity between hPCFT monomers and functional 'rescue' of mutant hPCFT by WT hPCFT [18]. hPCFT oligomers were also identified by Zhao et al. [21] by homobifunctional cross-linking with MTS-1-MTS and a putative TMD6 interface between hPCFT monomers was implied from the finding that MTS-1-MTS treatment generated cross-links between Cys^{229} (located in TMD6) in individual PCFT monomers, but not when Cys^{229} was mutated to serine.

The hPCFT primary sequence includes GXXXG motifs in TMD2 (amino acids 93–97) and in TMD4 (amino acids 155–159; Figure 1A), similar to dimerization motifs in other amphipathic proteins. GXXXG is one of the most frequently occurring transmembrane sequence motifs; the four-residue separation aligns the GXXXG glycines on one face of the helix, thus providing a flat surface for tight interactions between transmembrane α-helices [33–36]. The GXXXG motif has been linked to dimerization in membrane proteins [37–43]. While alanine substitution at Gly^{93} and Gly^{97} did not significantly affect hPCFT transport or oligomer formation [21], AXXXA motifs have also been reported to promote interactions between transmembrane helices [44].

To systematically investigate structural determinants of hPCFT oligomerization, in the present study, we characterized the roles of the $G^{93}XXXG^{97}$ and $G^{155}XXXG^{159}$ motifs in hPCFT expression and function, as well as in the formation of hPCFT oligomers, by comparing the impact of replacing glycines with alanines to that resulting from their replacement with leucines. Based on results of Zhao et al. [21] and molecular modelling, we also explored the roles of residues localized to TMDs 3 and 6 in forming critical structural interfaces between hPCFT monomers.

MATERIALS AND METHODS

Reagents

[3′,5′,7-^{3}H]Mtx (20 Ci/mmol) was purchased from Moravek Biochemicals. Unlabelled Mtx was provided by the Drug Development Branch, National Cancer Institute, National Institutes of Health. Synthetic oligonucleotides were obtained from Invitrogen. Tissue culture reagents and supplies were purchased from assorted vendors with the exception of FBS, which was purchased from Hyclone Technologies. The cross-linking reagent 1,6-hexanediyl *bis*methanethiosulfonate (MTS-6-MTS) was purchased from Toronto Research Chemicals.

Cell culture

The RFC- and hPCFT-null HeLa cell line, designated R1-11 [45], was a gift of Dr I. David Goldman (Bronx, NY). R1-11 cells were maintained in complete RPMI (Roswell Park Memorial Institute) 1640 medium containing 10% FBS, 2 mM L-glutamine, 100 units/ml penicillin and 100 μg/ml streptomycin [18].

hPCFT plasmid constructs and transient transfections

WT hPCFT constructs including *wt*^{FLAG}hPCFT$^{Myc\text{-}His10}$, *wt*hPCFT^{HA}, *wt*hPCFT^{Myc}, YPet–hPCFT and hPCFT–ECFP* were previously described [18]. WT Myc/HA-tagged hPCFT (*wt*hPCFT$^{Myc\text{-}HA}$) was prepared from *wt*hPCFT^{Myc} by removing the stop codon between the Myc and HA epitopes [18]. Glycine-to-leucine substitution mutants, including single (G93L, G97L, G155L, G159L) or multiple (G93L/G97L, G155L/G159L, G93L/G97L/G155L/G159L) leucine replacements, were prepared by site-directed mutagenesis, using *wt*hPCFT$^{Myc\text{-}HA}$, *wt*^{FLAG}hPCFT$^{Myc\text{-}His10}$, YPet–hPCFT and hPCFT–ECFP* [18] as templates. The analogous single and multiple glycine-to-alanine replacement mutants at positions 93, 97, 155 and 159 were generated in the same manner with *wt*^{FLAG}hPCFT$^{Myc\text{-}His10}$ as template. Cysteine-less (CL) hPCFT [30], including a HA epitope at the C-terminus (*cl*hPCFT^{HA}) in pCDNA3 was prepared by PCR from the hPCFT^{HA} construct [18], by mutagenizing Cys^{21}, Cys^{66}, Cys^{151}, Cys^{229}, Cys^{298}, Cys^{328} and Cys^{397} to serine, using the QuikChange™ Multi Site-Directed Mutagenesis Kit (Agilent) [30]. Single cysteine replacements were generated using *cl*hPCFT^{HA} as template and the QuikChange™ Site-Directed Mutagenesis Kit (Agilent). Primers were designed using the QuikChange™ Primer Design program (Agilent) and are available upon request. All mutations were confirmed by DNA sequencing by Genewiz, Inc.

WT and mutant hPCFT constructs (see below) were transiently transfected into R1-11 cells with Lipofectamine-Plus reagent (Invitrogen), as previously described [46]. With all transfections, cells were harvested after 48 h for transport and for preparing plasma membranes and Western blotting (see below). For experiments in which results for transfections with two plasmid constructs were directly compared with results for cells transfected with a single plasmid construct, constant DNA amounts were maintained by adding empty pCDNA3 (Invitrogen) to the single transfections.

Membrane transport experiments

Cellular uptake of [^{3}H]Mtx (0.5 μM) was measured over 2 min at 37°C in 60-mm dishes in MES-buffered saline (20 mM MES, 140 mM NaCl, 5 mM KCl, 2 mM $MgCl_2$ and 5 mM glucose) at pH 5.5 [15]. Levels of intracellular radioactivity were expressed as pmol/mg protein, calculated from direct measurements of radioactivity and protein contents [47] of the cell homogenates.

Membrane preparations and Western blot analysis of plasma membrane and cell surface hPCFT proteins

Plasma membrane preparations, SDS/PAGE and electrotransfer to polyvinylene difluoride membranes (Pierce) were exactly as reported previously [46]. Detection and quantification

of immunoreactive proteins used anti-hPCFT [18], anti-FLAG (Sigma), anti-HA (Covance) or anti-GFP (Abcam) antibodies and IRDye800-conjugated secondary antibody with an Odyssey® infrared imaging system (LI-COR). β-Actin was used as a loading control (Sigma).

For some experiments, the Cell Surface Labeling Accessory Pack (Thermo Scientific) was used to biotinylate and isolate surface membrane proteins prior to SDS/PAGE and Western analysis. Briefly, cells were incubated with 0.25 mg/ml sulfo-NHS (*N*-hydroxysuccinimide)-SS-biotin in PBS for 30 min at 4°C and then solubilized with lysis buffer. The lysates were centrifuged to remove the insoluble fraction. The supernatants were incubated with immobilized NeutrAvidin™ gel slurry for 1 h at room temperature, after which the beads were washed five times with wash buffer, containing protease inhibitors (Roche Applied Science). The proteins were eluted with 1× SDS/PAGE sample buffer [48], containing 50 mM DTT and analysed by SDS/PAGE/Western blotting.

Confocal microscopy and FRET analysis

For confocal microscopy, R1-11 cells were plated and transfected in Lab-Tek®II chamber slides (Nalge Nunc International). Cells were transfected with ECFP*-tagged WT and glycine-to-leucine mutant hPCFTs, then incubated with CellMask™ Deep Red plasma membrane stain (Invitrogen) for 5 min before being visualized with a Leica TCS SP5MP confocal microscope system, using a 63× oil immersion lens. The excitation/emission is 649/666 nm for the plasma membrane stain and 458/460–490 nm for ECFP*.

FRET analysis was performed exactly as in our previous report [18]. Briefly, R1-11 cells were seeded in 35-mm glass bottom micro well dishes (MatTek) 24 h before transfections with Lipofectamine-Plus reagents (see above), using 700 ng of DNA per dish (350 ng for each construct; for single transfections, 350 ng of pCDNA3 were added to maintain constant DNA). After 48 h and just prior to the FRET experiments, the medium was replaced with Leibovitz's L-15 medium (Invitrogen). Donor and acceptor images were acquired separately using a Leica TCS SP5MP confocal microscope system (Leica Microsystems), equipped with an argon laser (maximum luminous power at the focal plane is less than 30 milliwatts) with 458- and 514-nm lines. Spectral detection bandwidth of the Leica SP5 channels was set up to balance minimal cross-talk with optimal collection efficiency. FRET between YPet- and ECFP*-tagged hPCFT proteins was calculated using the FRET sensitized emission module of the Leica confocal software (LCS 2.61.1537), applying the equation: $FRET = (B - A \times \beta - C \times \gamma)/C$, where: A = ECFP* emission (by ECFP* excitation); B = FRET emission (by ECFP* excitation); C = YPet emission (by YPet excitation); β = correction factor for donor cross-talk (B/A when only ECFP* is expressed); and γ = correction factor for acceptor cross-excitation (B/C when only YPet is expressed) [18]. Positive and negative FRET controls include an ECFP*/YPet tandem construct and co-transfected separate ECFP* and YPet constructs, respectively [18]. FRET image raw data were processed using ImageJ software (W.S. Rasband, ImageJ, National Institutes of Health). The FRET experiments were performed in the Microscopy, Imaging, and Cytometry Resources Core at the Wayne State University School of Medicine.

Protein association study with histidine SpinTrap™ chromatography

R1-11 cells were co-transfected with FLAG/Myc-His_{10}– and HA-tagged WT or mutant hPCFTs as 1:1 ratios for both constructs. Transfected cells were harvested and disrupted (sonication) and membranes were solubilized by 1% *n*-dodecyl-*β*-D-maltoside for 2.5 h at 4°C. One-tenth of the solubilized samples was set aside as whole cell lysates to monitor protein expression levels by Western blots. The remainder was passed through His SpinTrap™ columns (GE Healthcare) with 20 mM sodium phosphate buffer (pH 7.4), containing 0.1% *n*-dodecyl-*β*-D-maltoside, 500 mM NaCl, EDTA-free proteinase inhibitor (Roche Applied Science) and 120 mM imidazole in both equilibration and washing buffers. The bound proteins were eluted with the above buffer, containing 500 mM imidazole [18]. The whole cell lysates and the eluted samples from the Ni^{2+}-chelating columns were fractionated on 4%–20% Tris/glycine gels (Invitrogen), followed by Western blotting.

Cross-linking of cysteine-substituted mutants of hPCFT

Forty-eight hours post-transfection with hPCFT mutants, R1-11 cells (in 60-mm dishes) were washed twice with Dulbecco's PBS and then treated with MTS-6-MTS [freshly dissolved in DMSO at 7.2 mg/ml (30 mM) and then diluted in PBS 1:100 (0.072 mg/ml or 0.3 mM)] on ice for 1 h. The cells were washed twice with PBS, then treated with 1.4 ml hypotonic buffer (0.5 mM Na_2HPO_4, 0.1 mM EDTA, pH 7.0) which contained protease inhibitor cocktail (Roche) on ice for 30 min. The cells were scraped from the dishes with rubber policemen and then centrifuged at 16 000 ***g*** at 4°C for 10 min. The cell pellets were solubilized in 0.4 ml of lysis buffer (50 mM Tris-base, 150 mM NaCl, 1% NP40 and 0.5% sodium deoxycholate, pH 7.4), then centrifuged (16 000 ***g***, 4°C) for 15 min to remove cell debris. The supernatant was frozen, protein contents determined [Bradford assay (Biorad)] and constant protein amounts were analysed by Western blotting using DTT-free 2× SDS/PAGE loading buffer.

Molecular modelling

Using the crystal structure of GlpT (1PW4) as template [49], we did homology modelling of the hPCFT monomer with Robetta Server (http://robetta.bakerlab.org). The top five hPCFT homology models retrieved through Robetta were evaluated by superimposing them over crystal structures of LacY, obtained at various states (1PV6, 1PV7, 2CFP, 2CFQ, 2V8N and 2Y5Y) and of GlpT (1PW4), by Chimera MatchMaker (http://www.cgl.ucsf.edu/chimera) with parameters optimized by superimposing GlpT (1PW4) over LacY (1PV6) that gave the lowest RMSD values over the longest Cα atoms. This was based on the notion that all crystal structures from three members (LacY, GlpT and EmrD) of the major facilitator superfamily (MFS) of transporters have preserved both secondary and tertiary structure elements during evolution [50]. The hPCFT model (hPCFT_R5) showing the lowest RMSD values (above) was manually adjusted with COOT (http://lmb.bioch.ox.ac.uk/coot/) to reflect the TMD2-3 re-entrant loop [30], resulting in hPCFT_R5_2-3RL. The hPCFT_R5_2-3RL model was further validated by assigning known residues that line the potential substrate binding pocket of hPCFT. The validated hPCFT_R5_2-3RL homology model was used to build an hPCFT dimeric model using MDOCK server [51], based on the notion that hPCFT forms oligomers with the dimer as dominant species [18].

Statistical analysis

Statistical analyses were performed using GraphPad 6.0 software.

RESULTS AND DISCUSSION

Characterization of the hPCFT $G^{93}XXXG^{97}$ and $G^{155}XXXG^{159}$ motifs by site-directed mutagenesis

hPCFT was reported to form homo-oligomers of which dimeric hPCFT was the predominant form [18]. However, structural determinants of hPCFT oligomerization have not been systematically studied. Analysis of the hPCFT amino acid sequence identified two GXXXG motifs, including a highly conserved sequence in TMD2 ($G^{93}XXXG^{97}$) and a lesser conserved sequence in TMD4 ($G^{155}XXXG^{159}$; Figure 1B). To interrogate these motifs for their possible roles in hPCFT oligomerization and transport function, we mutated glycine-to-leucine to generate single (G93L, G97L, G155L, G159L) and multiple (G93L/G97L, G155L/G159L, G93L/G97L/G155L/G159L) hPCFT mutants, using *wt*hPCFT$^{Myc\text{-}HA}$ as a template. WT and mutant hPCFT constructs were transiently transfected into hPCFT-null R1-11 cells and the transfected cells were assayed for membrane transport at pH 5.5 with [^{3}H]Mtx (0.5 μM) for 2 min at 37°C. Total hPCFT protein levels were measured in crude membranes, whereas cell surface expression of hPCFT protein was measured by surface biotinylation with sulfo-NHS-SS-biotin, followed by isolation of biotinylated proteins on immobilized NeutrAvidin™ gel. Crude membrane and biotinylated proteins were analysed by SDS/PAGE and Western blotting with HA-specific antibody.

Our results showed that for the G93L and G159L hPCFT mutants, substantial transport activity was preserved (35% and 69% of WT respectively; Figure 2, upper panel). Whereas transport for the other mutants was greatly diminished (particularly with the multiple leucine mutants), this was nonetheless significantly increased (5~15-fold; $P < 0.01$) over the low residual level measured in hPCFT-null R1-11 cells. Transport activity of the leucine replacement mutant proteins closely correlated with hPCFT protein levels in crude (Figure 2, middle panel) and surface (Figure 2, lower panel) membrane fractions, implying that the loss of transport function was probably due to impaired hPCFT trafficking and/or stability. On Western blots, both WT and mutant hPCFT proteins migrated as broad glycosylated species with unglycosylated bands at ~45 kDa. TMD GXXXG motifs were previously reported to serve critical roles in maintaining stability of the human organic anion transporter 1 [34]. The results with leucine-substitution mutants contrast with the corresponding glycine-to-alanine replacements at Gly^{93} and Gly^{97}, as reported by Zhao et al. [21] and as shown in Supplementary Figure S1 for G93A, G97A, G155A and G159A, for which expression and transport were largely preserved, although the G93A/G97A/G155A/G159A mutant was substantially impaired.

Analogous results were obtained for ECFP*-tagged WT and mutant hPCFT constructs based on *wt*hPCFT–ECFP* [18] in terms of relative transport activities (Figure 3A, upper panel) and hPCFT protein expression (Figure 3A, lower panels, shows Western blotting results for a crude membrane fraction analogous to that in Figure 2 probed with PCFT or GFP antibodies). By confocal microscopy, protein trafficking to the plasma membrane for

ECFP*-tagged WT, G93L and G159L hPCFTs was detected; however, for the G97L, G93L/G97L, G155L, G155L/G159L and G93L/G97L/G155L/G159L ECFP*-tagged mutants, fluorescence was mostly intracellular (Figure 3B), confirming a major effect on intracellular trafficking to the membrane surface.

Role of $G^{93}XXXG^{97}$ and $G^{155}XXXG^{159}$ motifs in hPCFT oligomerization

An important goal of our study was to test whether leucine-for-glycine replacements in the GXXXG motifs in TMD2 ($G^{93}XXXG^{97}$) and TMD4 ($G^{155}XXXG^{159}$) impacted hPCFT oligomerization, given previous reports of a role of GXXXG motifs in membrane protein oligomerization [37–43]. If so, this would implicate these regions as structurally important for forming hPCFT oligomers. We previously used Ni^{2+}-chelating chromatography to assay associations between co-expressed Myc-His_{10} and HA-tagged hPCFT monomers [18]. In the present study, we used this approach to study associations between co-expressed Myc-HA-tagged hPCFT (Figure 2) and FLAG/Myc-His_{10}-tagged hPCFT [18], including both WT and glycine-to-leucine mutant proteins. Again, the mutant proteins included single (G93L, G97L, G155L, G159L) and multiple (G93L/G97L, G155L/G159L, G93L/G97L/G155L/G159L) leucine-for-glycine replacements. WT and mutant ^{FLAG}hPCFT$^{Myc\text{-}his10}$ proteins were characterized for their transport activity (Figure 4A, upper panel) and membrane expression (Figure 4A, lower panel) which generally paralleled results with Myc-HA-tagged hPCFT forms (Figure 2).

We first studied co-associations for individual glycine-to-leucine mutants by Ni^{2+} chelating chromatography (i.e., HisSpinTrap™) using co-expressed (hPCFT$^{Myc\text{-}HA}$ plus ^{FLAG}hPCFT$^{Myc\text{-}His10}$) constructs for each form. WT hPCFT constructs were included as controls. As additional controls, single transfectants (hPCFT$^{Myc\text{-}HA}$ or ^{FLAG}hPCFT$^{Myc\text{-}His10}$ for each form) were individually expressed and mixed together just prior to chromatography (labelled ‘mix’ in Figure 4B). Total cell proteins were solubilized with 1% *n*-dodecyl-*β*-D-maltoside, followed by fractionation on HisSpinTrap™ affinity columns and Western blot analysis with epitope-specific antibodies. When extracts from singly transfected samples of WT or mutant proteins were mixed just prior to chromatography, only the ^{FLAG}hPCFT$^{Myc\text{-}His10}$ proteins (but not hPCFT$^{Myc\text{-}HA}$) bound to the columns (Figure 4B, lanes 2, 4, 6, 8, 10, 12, 14, 16). When *wt*^{FLAG}hPCFT$^{Myc\text{-}His10}$ and *wt*hPCFT$^{Myc\text{-}HA}$ proteins were co-expressed in R1-11 cells, both forms were retained on the nickel columns and were detected with FLAG and HA antibodies, respectively (Figure 4B, lane 3). Analogous results were obtained for the individual glycine-to-leucine mutants (Figure 4B, lanes 5, 7, 9, 11, 13, 15 and 17). Thus, glycine-to-leucine mutations of hPCFT GXXXG motifs did not interfere with co-associations between individual mutant proteins.

We tested the associations between FLAG/Myc-His_{10}-tagged WT hPCFT and the individual Myc-HA-tagged glycine-to-leucine mutants in co-expression experiments with R1-11 cells, followed by Ni^{2+} chromatography (Figure 4C). We co-expressed *wt*^{FLAG}hPCFT$^{Myc\text{-}His10}$ and *wt*hPCFT$^{Myc\text{-}HA}$ proteins as a positive control (lanes 2 and 3). For the mutants co-expressed with WT hPCFT, again both FLAG/Myc-His_{10}-tagged WT and Myc-HA tagged glycine-to-leucine mutant proteins were retained on the nickel columns (Figure 4C, lanes 5, 7, 9, 11, 13, 15 and 17) and none of the Myc-HA-tagged glycine-to-leucine mutant proteins

were detected in the 'mixed' samples (Figure 4C, lanes 4, 6, 8, 10, 12, 14 and 16). These results establish that the glycine-to-leucine GXXXG mutations in TMD2 and TMD4 do not interfere with associations between WT and mutant monomers.

We extended our studies of hPCFT oligomerization *in situ* by FRET. Since the association between monomeric hPCFT molecules showed a preferential ('head-to-tail') orientation [18], we used N-terminal YPet- and C-terminal-ECFP*-tagged (above) WT and GXXXG glycine-to-leucine mutant constructs for these experiments. The YPet-tagged hPCFT mutants expressed in R1-11 cells showed similar patterns of [^{3}H]Mtx transport and hPCFT expression to the Myc-HA-tagged and ECFT*-tagged hPCFT proteins (compare Supplementary Figure S2 and Figures 2 and 3A).

To measure FRET, R1-11 cells were co-transfected with YPet-and ECFP*-tagged WT or glycine-to-leucine mutant constructs. As controls, cells were transfected with combined YPet and ECFP* constructs (negative control) and with an YPet-ECFP* tandem construct (positive control). Sensitized emission FRET was used and images were collected in the FRET channel and corrected for fluorescence bleed-through. Representative FRET images are shown in Figure 5. Calculated FRET values of both test samples and controls are represented using a pseudo colour-scale. Figure 5 shows FRET for the YPet–ECFP* positive control (B), the YPet–hPCFT WT plus hPCFT–ECFP* WT (C) and for all glycine-to-leucine mutant (D–J) constructs, at levels far exceeding that for the YPet plus ECFP* negative control (a). This establishes close proximity (within 100 Å) of the fluorescent-tagged hPCFT monomers of the glycine-to-leucine mutants. For the YPet- and ECFP*-tagged WT and the G93L and G159L mutant constructs, the majority of FRET was unambiguously localized to the cell surface. However, there was appreciable intracellular FRET for other glycine-to-leucine mutants, consistent with the intracellular association between hPCFT monomers and findings of intracellular hPCFT by indirect immunofluorescence staining (Figure 3B). These results strongly support the notion that hPCFT oligomers of glycine-to-leucine mutants form *in situ*. Since FRET was detected for both surface and intracellular glycine-to-leucine mutants, it was very likely that oligomerization of hPCFT is not required for surface targeting.

TMDs 3 and 6 form a boundary between monomeric hPCFT

A role for Cys^{229} (in TMD6) in hPCFT oligomerization was previously implied from the finding that mutation of Cys^{229} to serine abolished cross-linking with MTS-1-MTS [21]. Using GlpT as a template [49] and based on published studies for hPCFT [20–24,26–28,30,52], we generated a 3D homology model for monomeric hPCFT in which TMDs 1, 2, 4, 5, 7, 8, 10 and 11 comprise an aqueous transmembrane pathway, flanked by TMDs 3, 6, 9 and 12 (Figures 6A and 6B). With MDOCK modelling [51] of this hPCFT monomer structure, a dimeric hPCFT structure was predicted (Figure 6C) with juxtaposed TMDs 2, 3, 4 and 6 as structural interfaces between hPCFT monomers, analogous to other oligomeric MFS proteins [53–55].

To begin to test this model and to extend the published results of Zhao et al. [21], we inserted cysteine residues into a *cl*hPCFT^{HA} background [30] from positions 115–137 spanning TMD3 and from positions 213–236 spanning TMD6. Individual cysteine mutant

constructs were transfected into R1-11 cells and after 48 h, transfected cells were assayed for hPCFT protein levels in crude membranes by SDS/PAGE and Western blotting (Figures 7A and 7B, lower panels) and for transport at pH 5.5 with [^{3}H]Mtx (0.5 μM) (Figure 7A and B, upper panels). Most of the cysteine-insertion mutants preserved substantial transport activity and only G123C, V130C, E232C and T233C were functionally inert (<2-fold increased over R1-11 cells; noted with asterisks in Figures 7A and 7B).

The active cysteine mutants in TMDs 3 and 6 were cross-linked with MTS-6-MTS cross-linker and analysed on Western blots. Cys^{229}-hPCFT formed cross-links, as reflected in slowly migrating high molecular mass (~90 kDa) hPCFT species not seen with *cl*hPCFT^{HA} or non-cross-linked S229C (Figure 7C, upper panel). Distinct cross-linked species were also formed for the Q136C and L137C mutants in TMD3 (Figure 7C, middle panel) and for the W213C, L214C, L224C, A227C, F228C, F230C and G231C hPCFT mutants in TMD6 (Figure 7C, lower panel). Again, no similar higher molecular mass species were detected in the absence of cross-linker (Figures 7A and 7B, lower panels).

These results establish the proximities between vicinal residues localized in the exofacial end of TMD3 and in the exofacial and cytosolic ends of TMD6, consistent with the notion that these stretches of amino acids form structural interfaces between hPCFT monomers, as suggested by the molecular model in Figure 6(C).

CONCLUSIONS

hPCFT forms homo-oligomers that are functionally important [18]. In the present study, we systematically interrogated potential structural determinants of hPCFT monomer associations in the formation of hPCFT oligomers. Putative GXXXG dimerization motifs were identified in TMDs 2 and 4 of hPCFT and published cross-linking results previously implied an important role for TMD6 in forming a critical interface between hPCFT monomers [21].

We used leucine-for-glycine replacements at Gly^{93}, Gly^{97}, Gly^{155} and Gly^{159} which should disrupt the putative GXXXG motifs if they were structurally or functionally important. This resulted in substantial losses of transport activity for many of the mutants (for G97L, G93L/G97L, G155L, G155L/G159L and G93L/G97L/G155L/G159L), although G93L and G159L retained substantial transport function compared with WT hPCFT. For most of the glycine-to-leucine mutants, losses of transport were accompanied by dramatically decreased levels of hPCFT protein including both total membrane and surface hPCFT. This suggests that the principal role for the GXXXGs in TMDs 2 and 4 of hPCFT is to facilitate intramolecular packing and protein stability of transmembrane α helices analogous to other transporters [34–36]. However, there was no evidence that disruption of G^{93}XXXG^{97} or G^{155}XXXG^{159} motifs affected monomer associations in forming hPCFT oligomers by Ni^{2+}-affinity chromatography and *in situ* FRET assays. With G^{93}XXXG^{97} and G^{155}XXXG^{159}, the single glycine-to-alanine replacement mutants were all expressed and showed high levels of transport, although transport decreased somewhat for the multiple alanine mutants. These results indicate that alanine is able to replace glycine without appreciably interfering with protein function and would probably preserve analogous interactions between

transmembrane helices required for transport [34–36,56]. Our finding that Gly^{93} is unlikely to participate in hPCFT oligomerization is consistent with the finding that Gly^{93} and Phe^{94} contribute to a substrate binding domain, based on results of substituted cysteine-accessibility studies [30].

Our cross-linking results implicated TMDs 3 and 6 as forming critical monomer interfaces in homo-oligomeric hPCFT since homobifunctional cross-linking of cysteine-insertion mutants across these stretches established the proximities between these individual TMDs. These results directly support molecular modelling results which predict that TMDs 2, 3, 4 and 6 form critical interfaces between hPCFT monomers. Based on these results, experiments are underway to further define the minimal determinants for hPCFT oligomerization. Identification of structural motifs or domains involved in hPCFT oligomerization may lead to novel approaches for therapeutically 'rescuing' functionally impaired hPCFT mutants or for enhancing surface expression of hPCFT in tumours treated with hPCFT-selective anti-folates.

Supplementary Material

Refer to Web version on PubMed Central for supplementary material.

Acknowledgments

We thank Dr I. David Goldman for a generous gift of RFC- and hPCFT-null R1-11 HeLa cells. We thank Dr Tomoo Ohashi (Duke University Medical Center) for providing the YPet-His and ECFP*-His cDNAs for the FRET experiments.

FUNDING

This study was supported by grants from National Institutes of Health including R01 CA53535 (to L.H.M. and Z.H.) and P30CA22453 (Karmanos Cancer Institute), and contract number HSN275201300006C (Perinatology Research Branch of NICHD, NIH, Wayne State University). Mr. Wilson was supported by National Institutes of Health Training Grant T32 CA009531 (to L.H.M).

Abbreviations

cl	cysteine-less
ECFP*	enhanced cyan fluorescent protein with K26R/N164H mutation
HA	haemagglutinin
hPCFT	human PCFT
MFS	major facilitator superfamily
MTS-1-MTS	1,1-methanediyl *bis*methanethiosulfonate
MTS-6-MTS	1,6-hexanediyl *bis*methanethiosulfonate
Mtx	methotrexate
PCFT	proton-coupled folate transporter
Pmx	pemetrexed

RFC	reduced folate carrier
sulfo-NHS-SS-biotin	sulfo-*N*-hydroxysuccinimide-SS-biotin
TMD	transmembrane domain
WT	wild-type
YPet	FRET-optimized yellow fluorescent protein

References

1. Stokstad, ELR. Historical perspective on key advances in the biochemistry and physiology of folates. In: Picciano, MF.; Stokstad, ELR.; Greogory, JF., editors. Contemporory Issues in Clinical Nutrition: Folic Acid Metabolism in Health and Diesease. Wiley-Liss; New York: 1990. p. 1-21.
2. Zhao R, Diop-Bove N, Visentin M, Goldman ID. Mechanisms of membrane transport of folates into cells and across epithelia. Annu Rev Nutr. 2011; 31:177–201. [PubMed: 21568705]
3. Matherly LH, Wilson MR, Hou Z. The Major facilitative folate transporters solute carrier 19A1 and solute carrier 46A1: biology and role in antifolate chemotherapy of cancer. Drug Metab Dispos. 2014; 42:632–649. [PubMed: 24396145]
4. Zhao R, Matherly LH, Goldman ID. Membrane transporters and folate homeostasis: intestinal absorption and transport into systemic compartments and tissues. Expert Rev Mol Med. 2009; 11:e4. [PubMed: 19173758]
5. Chattopadhyay S, Tamari R, Min SH, Zhao R, Tsai E, Goldman ID. Commentary: a case for minimizing folate supplementation in clinical regimens with pemetrexed based on the marked sensitivity of the drug to folate availability. Oncologist. 2007; 12:808–815. [PubMed: 17673612]
6. Nakai Y, Inoue K, Abe N, Hatakeyama M, Ohta KY, Otagiri M, Hayashi Y, Yuasa H. Functional characterization of human proton-coupled folate transporter/heme carrier protein 1 heterologously expressed in mammalian cells as a folate transporter. J Pharmacol Exp Ther. 2007; 322:469–476. [PubMed: 17475902]
7. Qiu A, Jansen M, Sakaris A, Min SH, Chattopadhyay S, Tsai E, Sandoval C, Zhao R, Akabas MH, Goldman ID. Identification of an intestinal folate transporter and the molecular basis for hereditary folate malabsorption. Cell. 2006; 127:917–928. [PubMed: 17129779]
8. Desmoulin SK, Hou Z, Gangjee A, Matherly LH. The human proton-coupled folate transporter: Biology and therapeutic applications to cancer. Cancer Biol Ther. 2012; 13:1355–1373. [PubMed: 22954694]
9. Kugel Desmoulin S, Wang L, Hales E, Polin L, White K, Kushner J, Stout M, Hou Z, Cherian C, Gangjee A, Matherly LH. Therapeutic targeting of a novel 6-substituted pyrrolo [2,3-d]pyrimidine thienoyl antifolate to human solid tumors based on selective uptake by the proton-coupled folate transporter. Mol Pharmacol. 2011; 80:1096–1107. [PubMed: 21940787]
10. Zhao R, Gao F, Hanscom M, Goldman ID. A prominent low-pH methotrexate transport activity in human solid tumors: contribution to the preservation of methotrexate pharmacologic activity in HeLa cells lacking the reduced folate carrier. Clin Cancer Res. 2004; 10:718–727. [PubMed: 14760095]
11. Deng Y, Zhou X, Kugel Desmoulin S, Wu J, Cherian C, Hou Z, Matherly LH, Gangjee A. Synthesis and biological activity of a novel series of 6-substituted thieno[2,3-d]pyrimidine antifolate inhibitors of purine biosynthesis with selectivity for high affinity folate receptors over the reduced folate carrier and proton-coupled folate transporter for cellular entry. J Med Chem. 2009; 52:2940–2951. [PubMed: 19371039]
12. Cherian C, Kugel Desmoulin S, Wang L, Polin L, White K, Kushner J, Stout M, Hou Z, Gangjee A, Matherly LH. Therapeutic targeting malignant mesothelioma with a novel 6-substituted pyrrolo[2,3-d]pyrimidine thienoyl antifolate via its selective uptake by the proton-coupled folate transporter. Cancer Chemother Pharmacol. 2013; 71:999–1011. [PubMed: 23412628]

13. Kugel Desmoulin S, Hou Z, Gangjee A, Matherly LH. The human proton-coupled folate transporter: Biology and therapeutic applications to cancer. Cancer Biol Therapy. 2012; 13:1355–1373.

14. Kugel Desmoulin S, Wang L, Polin L, White K, Kushner J, Stout M, Hou Z, Cherian C, Gangjee A, Matherly LH. Functional loss of the reduced folate carrier enhances the antitumor activities of novel antifolates with selective uptake by the proton-coupled folate transporter. Mol Pharmacol. 2012; 82:591–600. [PubMed: 22740639]

15. Kugel Desmoulin S, Wang Y, Wu J, Stout M, Hou Z, Fulterer A, Chang MH, Romero MF, Cherian C, Gangjee A, Matherly LH. Targeting the proton-coupled folate transporter for selective delivery of 6-substituted pyrrolo[2,3-d]pyrimidine antifolate inhibitors of *de novo* purine biosynthesis in the chemotherapy of solid tumors. Mol Pharmacol. 2010; 78:577–587. [PubMed: 20601456]

16. Wang L, Cherian C, Kugel Desmoulin S, Polin L, Deng Y, Wu J, Hou Z, White K, Kushner J, Matherly LH, Gangjee A. Synthesis and antitumor activity of a novel series of 6-substituted pyrrolo[2,3-d]pyrimidine thienoyl antifolate inhibitors of purine biosynthesis with selectivity for high affinity folate receptors and the proton-coupled folate transporter over the reduced folate carrier for cellular entry. J Med Chem. 2010; 53:1306–1318. [PubMed: 20085328]

17. Wang L, Kugel Desmoulin S, Cherian C, Polin L, White K, Kushner J, Fulterer A, Chang MH, Mitchell-Ryan S, Stout M, et al. Synthesis, biological, and antitumor activity of a highly potent 6-substituted pyrrolo[2,3-d]pyrimidine thienoyl antifolate inhibitor with proton-coupled folate transporter and folate receptor selectivity over the reduced folate carrier that inhibits beta-glycinamide ribonucleotide formyltransferase. J Med Chem. 2011; 54:7150–7164. [PubMed: 21879757]

18. Hou Z, Kugel Desmoulin S, Etnyre E, Olive M, Hsiung B, Cherian C, Wloszczynski PA, Moin K, Matherly LH. Identification and functional impact of homo-oligomers of the human proton-coupled folate transporter. J Biol Chem. 2012; 287:4982–4995. [PubMed: 22179615]

19. Hou Z, Matherly LH. Biology of the major facilitative folate transporters SLC19A1 and SLC46A1. Curr Top Membr. 2014; 73:175–204. [PubMed: 24745983]

20. Shin DS, Zhao R, Fiser A, Goldman ID. Role of the fourth transmembrane domain in proton-coupled folate transporter function as assessed by the substituted cysteine accessibility method. Am J Physiol Cell Physiol. 2013; 304:C1159–C1167. [PubMed: 23552283]

21. Zhao R, Shin DS, Fiser A, Goldman ID. Identification of a functionally critical GXXG motif and its relationship to the folate binding site of the proton-coupled folate transporter (PCFT-SLC46A1). Am J Physiol Cell Physiol. 2012; 303:C673–C681. [PubMed: 22785121]

22. Mahadeo K, Diop-Bove N, Shin D, Unal ES, Teo J, Zhao R, Chang MH, Fulterer A, Romero MF, Goldman ID. Properties of the Arg376 residue of the proton-coupled folate transporter (PCFT-SLC46A1) and a glutamine mutant causing hereditary folate malabsorption. Am J Physiol Cell Physiol. 2010; 299:C1153–C1161. [PubMed: 20686069]

23. Unal ES, Zhao R, Chang MH, Fiser A, Romero MF, Goldman ID. The functional roles of the His247 and His281 residues in folate and proton translocation mediated by the human proton-coupled folate transporter SLC46A1. J Biol Chem. 2009; 284:17846–17857. [PubMed: 19389703]

24. Unal ES, Zhao R, Goldman ID. Role of the glutamate 185 residue in proton translocation mediated by the proton-coupled folate transporter SLC46A1. Am J Physiol Cell Physiol. 2009; 297:C66–C74. [PubMed: 19403800]

25. Zhao R, Min SH, Qiu A, Sakaris A, Goldberg GL, Sandoval C, Malatack JJ, Rosenblatt DS, Goldman ID. The spectrum of mutations in the PCFT gene, coding for an intestinal folate transporter, that are the basis for hereditary folate malabsorption. Blood. 2007; 110:1147–1152. [PubMed: 17446347]

26. Lasry I, Berman B, Straussberg R, Sofer Y, Bessler H, Sharkia M, Glaser F, Jansen G, Drori S, Assaraf YG. A novel loss-of-function mutation in the proton-coupled folate transporter from a patient with hereditary folate malabsorption reveals that Arg 113 is crucial for function. Blood. 2008; 112:2055–2061. [PubMed: 18559978]

27. Shin DS, Min SH, Russell L, Zhao R, Fiser A, Goldman ID. Functional roles of aspartate residues of the proton-coupled folate transporter (PCFT-SLC46A1); a D156Y mutation causing hereditary folate malabsorption. Blood. 2010; 116:5162–5169. [PubMed: 20805364]

28. Zhao R, Shin DS, Diop-Bove N, Ovits CG, Goldman ID. Random mutagenesis of the proton-coupled folate transporter (SLC46A1), clustering of mutations, and the bases for associated losses of function. J Biol Chem. 2011; 286:24150–24158. [PubMed: 21602279]
29. Shin DS, Zhao R, Yap EH, Fiser A, Goldman ID. A P425R mutation of the proton-coupled folate transporter causing hereditary folate malabsorption produces a highly selective alteration in folate binding. American journal of physiology Cell Physiol. 2012; 302:C1405–C1412.
30. Wilson MR, Hou Z, Matherly LH. Substituted cysteine accessibility reveals a novel transmembrane 2–3 reentrant loop and functional role for transmembrane domain 2 in the human proton-coupled folate transporter. J Biol Chem. 2014; 289:25287–25295. [PubMed: 25053408]
31. Unal ES, Zhao R, Qiu A, Goldman ID. N-linked glycosylation and its impact on the electrophoretic mobility and function of the human proton-coupled folate transporter (HsPCFT). Biochim Biophys Acta. 2008; 1778:1407–1414. [PubMed: 18405659]
32. Subramanian VS, Marchant JS, Said HM. Apical membrane targeting and trafficking of the human proton-coupled transporter in polarized epithelia. Am J Physiol Cell Physiol. 2008; 294:C233–C240. [PubMed: 18003745]
33. Mueller BK, Subramaniam S, Senes A. A frequent, GxxxG-mediated, transmembrane association motif is optimized for the formation of interhelical Calpha-H hydrogen bonds. Proc Natl Acad Sci USA. 2014; 111:E888–E895. [PubMed: 24569864]
34. Duan P, Wu J, You G. Mutational analysis of the role of GXXXG motif in the function of human organic anion transporter 1 (hOAT1). Int J Biochem Mol Biol. 2011; 2:1–7. [PubMed: 21340049]
35. Russ WP, Engelman DM. The GxxxG motif: a framework for transmembrane helix-helix association. J Mol Biol. 2000; 296:911–919. [PubMed: 10677291]
36. Polgar O, Robey RW, Morisaki K, Dean M, Michejda C, Sauna ZE, Ambudkar SV, Tarasova N, Bates SE. Mutational analysis of ABCG2: role of the GXXXG motif. Biochemistry. 2004; 43:9448–9456. [PubMed: 15260487]
37. Gerber D, Shai Y. *In vivo* detection of hetero-association of glycophorin-A and its mutants within the membrane. J Biol Chem. 2001; 276:31229–31232. [PubMed: 11402026]
38. Whittington DA, Waheed A, Ulmasov B, Shah GN, Grubb JH, Sly WS, Christianson DW. Crystal structure of the dimeric extracellular domain of human carbonic anhydrase XII, a bitopic membrane protein overexpressed in certain cancer tumor cells. Proc Natl Acad Sci USA. 2001; 98:9545–9550. [PubMed: 11493685]
39. Melnyk RA, Partridge AW, Deber CM. Transmembrane domain mediated self-assembly of major coat protein subunits from Ff bacteriophage. J Mol Biol. 2002; 315:63–72. [PubMed: 11771966]
40. Arselin G, Giraud MF, Dautant A, Vaillier J, Brethes D, Coulary-Salin B, Schaeffer J, Velours J. The GxxxG motif of the transmembrane domain of subunit e is involved in the dimerization/oligomerization of the yeast ATP synthase complex in the mitochondrial membrane. Eur J Biochem. 2003; 270:1875–1884. [PubMed: 12694201]
41. McClain MS, Iwamoto H, Cao P, Vinion-Dubiel AD, Li Y, Szabo G, Shao Z, Cover TL. Essential role of a GXXXG motif for membrane channel formation by *Helicobacter pylori* vacuolating toxin. J Biol Chem. 2003; 278:12101–12108. [PubMed: 12562777]
42. Overton MC, Chinault SL, Blumer KJ. Oligomerization, biogenesis, and signaling is promoted by a glycophorin A-like dimerization motif in transmembrane domain 1 of a yeast G protein-coupled receptor. J Biol Chem. 2003; 278:49369–49377. [PubMed: 14506226]
43. Mendrola JM, Berger MB, King MC, Lemmon MA. The single transmembrane domains of ErbB receptors self-associate in cell membranes. J Biol Chem. 2002; 277:4704–4712. [PubMed: 11741943]
44. Kleiger G, Grothe R, Mallick P, Eisenberg D. GXXXG and AXXXA: common alpha-helical interaction motifs in proteins, particularly in extremophiles. Biochemistry. 2002; 41:5990–5997. [PubMed: 11993993]
45. Diop-Bove NK, Wu J, Zhao R, Locker J, Goldman ID. Hypermethylation of the human proton-coupled folate transporter (SLC46A1) minimal trancriptional regulatory region in an antifolate-resistant HeLa cell line. Mol Cancer Ther. 2009; 8:2424–2431. [PubMed: 19671745]

46. Hou Z, Stapels SE, Haska CL, Matherly LH. Localization of a substrate binding domain of the human reduced folate carrier to transmembrane domain 11 by radioaffinity labeling and cysteine-substituted accessibility methods. J Biol Chem. 2005; 280:36206–36213. [PubMed: 16115875]
47. Lowry OH, Rosebrough NJ, Farr AL, Randall RJ. Protein measurement with the Folin phenol reagent. J Biol Chem. 1951; 193:265–275. [PubMed: 14907713]
48. Laemmli UK. Cleavage of structural proteins during the assembly of the head of bacteriophage T4. Nature. 1970; 227:680–685. [PubMed: 5432063]
49. Huang Y, Lemieux MJ, Song J, Auer M, Wang DN. Structure and mechanism of the glycerol-3-phosphate transporter from *Escherichia coli*. Science. 2003; 301:616–620. [PubMed: 12893936]
50. Abramson J, Kaback HR, Iwata S. Structural comparison of lactose permease and the glycerol-3-phosphate antiporter: members of the major facilitator superfamily. Curr Opin Struct Biol. 2004; 14:413–419. [PubMed: 15313234]
51. Pierce BG, Wiehe K, Hwang H, Kim BH, Vreven T, Weng Z. ZDOCK server: interactive docking prediction of protein-protein complexes and symmetric multimers. Bioinformatics. 2014; 30:1771–1773. [PubMed: 24532726]
52. Lasry I, Berman B, Glaser F, Jansen G, Assaraf YG. Hereditary folate malabsorption: a positively charged amino acid at position 113 of the proton-coupled folate transporter (PCFT/SLC46A1) is required for folic acid binding. Biochem Biophys Res Commun. 2009; 386:426–431. [PubMed: 19508863]
53. Scholze P, Freissmuth M, Sitte HH. Mutations within an intramembrane leucine heptad repeat disrupt oligomer formation of the rat GABA transporter 1. J Biol Chem. 2002; 277:43682–43690. [PubMed: 12223478]
54. Korkhov VM, Farhan H, Freissmuth M, Sitte HH. Oligomerization of the {gamma}-aminobutyric acid transporter-1 is driven by an interplay of polar and hydrophobic interactions in transmembrane helix II. J Biol Chem. 2004; 279:55728–55736. [PubMed: 15496410]
55. Sitte HH, Farhan H, Javitch JA. Sodium-dependent neurotransmitter transporters: oligomerization as a determinant of transporter function and trafficking. Mol Interv. 2004; 4:38–47. [PubMed: 14993475]
56. Senes A, Engel DE, DeGrado WF. Folding of helical membrane proteins: the role of polar, GxxxG-like and proline motifs. Curr Opin Struct Biol. 2004; 14:465–479. [PubMed: 15313242]

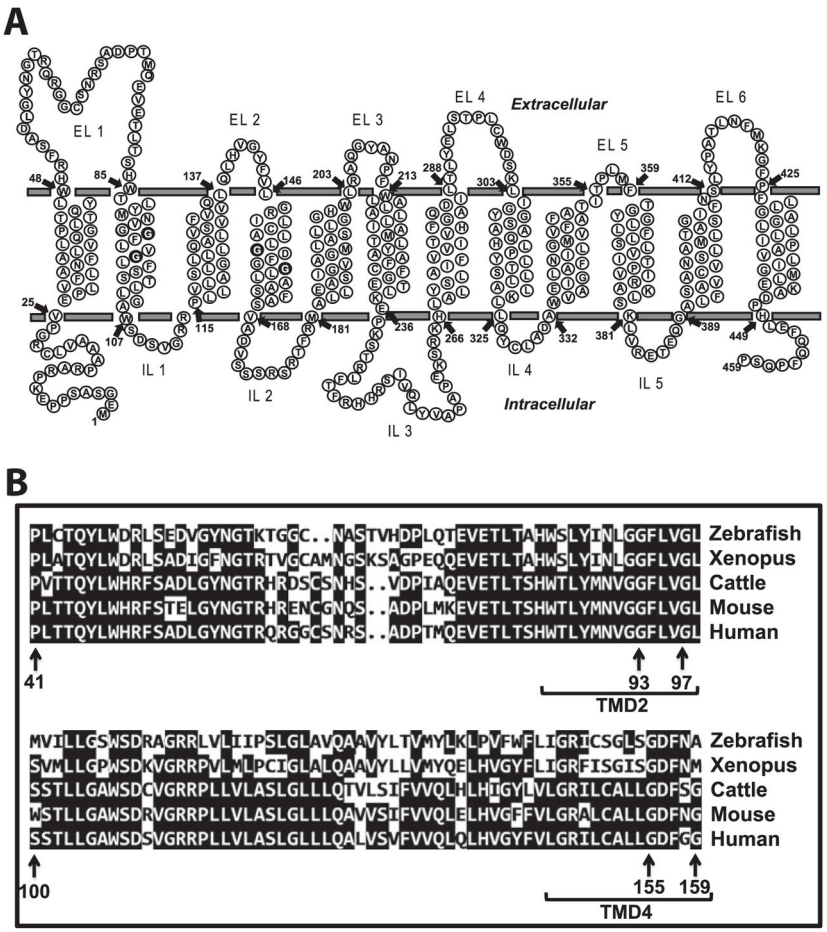

Figure 1. Schematic structure of hPCFT membrane topology and partial sequence alignment of PCFT homologues

(**A**) A topology model is shown for human PCFT, with 12 TMDs and internal N- and C-termini. Glycines (at positions of 93, 97, 155 and 159) constituting GXXXG putative oligomerization motifs are shown as black circles. TMDs 3 (residues 115–137) and 6 (residues 213–236) were implicated as forming PCFT oligomer interfaces in this study. (**B**) Alignment of sequence containing GXXXG motifs of PCFT homologues from different species is shown. The first such motif in hPCFT TMD2 ($G^{93}XXXG^{97}$) is more conserved than the motif in hPCFT TMD4 ($G^{155}XXXG^{159}$). Partial sequences of hPCFT TMD2 and 4 that include GXXXG motifs are noted.

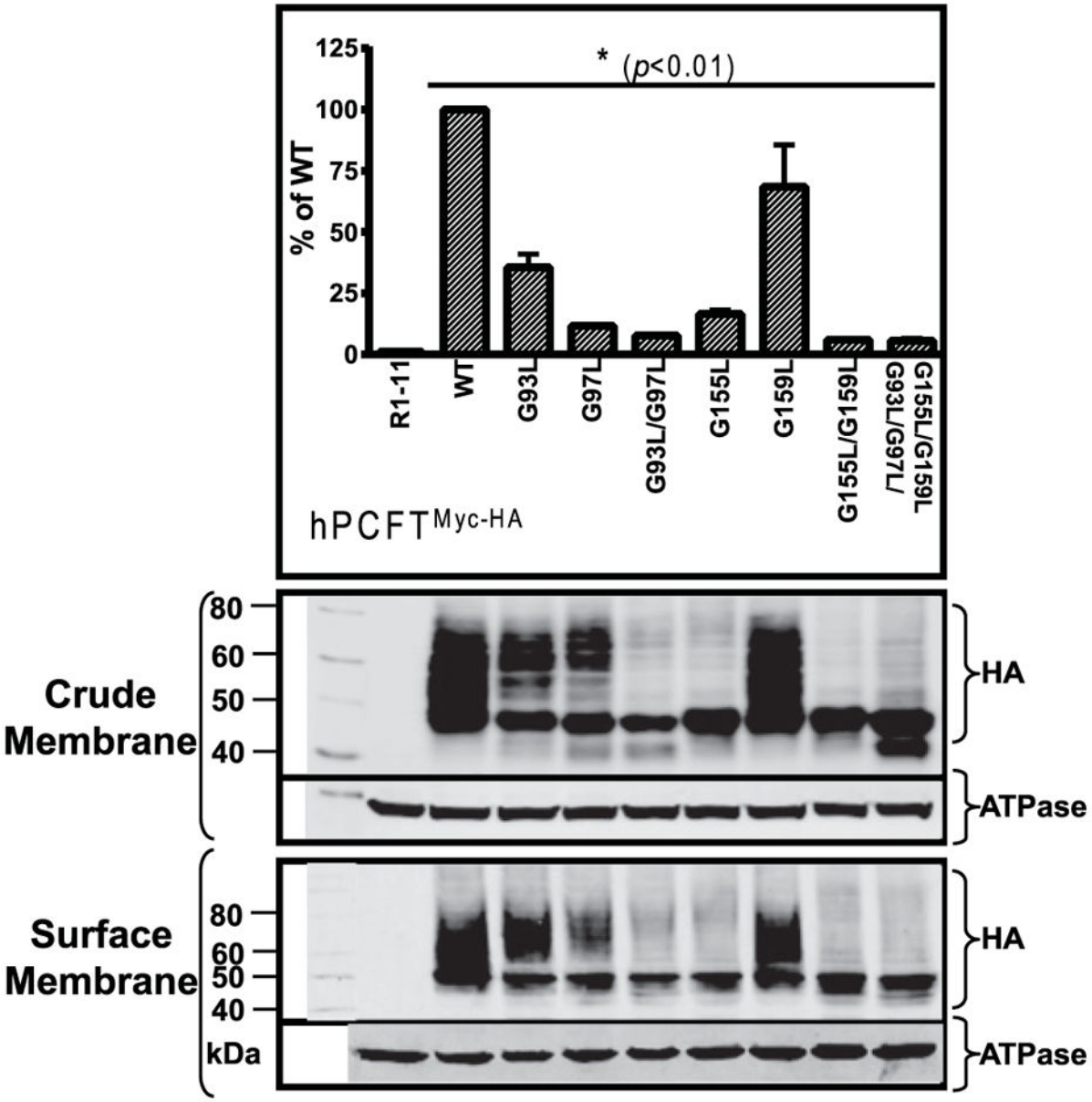

Figure 2. Transport function and protein expression of glycine-to-leucine mutants of hPCFT^{Myc-HA}

To investigate the role of the GXXXG motifs in hPCFT oligomerization, we mutated glycine-to-leucine to obtain single (G93L, G97L, G155L, G159L) or multiple (G93L/G97L, G155L/G159L, G93L/G97L/G155L/G159L) mutants, based on *wt*hPCFT^{Myc-HA}. hPCFT WT and glycine-to-leucine mutants were transiently transfected into hPCFT-null R1-11 cells. Transfected cells were assayed for transport at pH 5.5 with [^{3}H]Mtx (0.5 μM) for 2 min at 37°C (upper panel). hPCFT protein expression was measured in crude membranes by SDS/PAGE and Western blotting with HA antibody (middle panel). hPCFT protein expression at the cell surface [labelled with sulfo-NHS-SS-biotin (0.25 mg/ml) and isolated on immobilized NeutrAvidin™ gel] was also measured and probed with HA antibody (lower panel). Na^+/K^+ ATPase was used as a loading control. The molecular mass markers for

SDS/PAGE are noted. Transport results are expressed relative to those for WT hPCFT$^{Myc\text{-}HA}$ and are reported as mean values ± standard errors from four independent experiments. The transport differences between non-transfected R1-11 cells and R1-11 cells transfected with WT and glycine-to-leucine mutant hPCFTs were statistically significant (*$P < 0.01$).

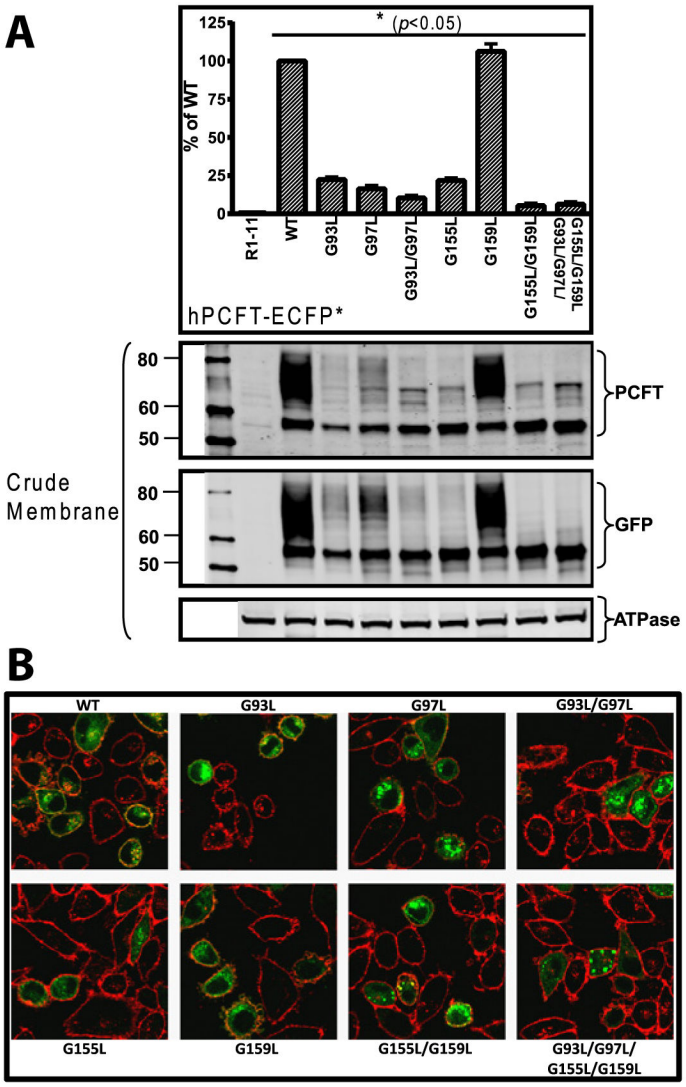

Figure 3. Transport function and protein expression of WT glycine-to-leucine mutants of hPCFT–ECFP*

To localize the expression of WT and glycine-to-leucine mutant hPCFT proteins, we mutated glycine-to-leucine to obtain single (G93L, G97L, G155L, G159L) or multiple (G93L/G97L, G155L/G159L, G93L/G97L/G155L/G159L) mutants, based on *wt*hPCFT-ECFP*. (**A**) hPCFT WT and glycine-to-leucine mutants were transiently transfected into hPCFT-null R1-11 cells. Transfected cells were assayed for transport at pH 5.5 with [^{3}H]Mtx (0.5 μM) for 2 min at 37°C (upper panel). hPCFT protein expression was measured in crude membranes by SDS/PAGE and Western blotting with hPCFT antibody (middle panel) or GFP antibody (lower panel). Na^+/K^+ ATPase was used as a loading control. The molecular mass markers for SDS/PAGE are noted (in kDa). Transport results are expressed relative to those for WT hPCFT–ECFP* and are reported as mean values ± standard errors from three independent experiments. The transport differences between non-transfected and transfected R1-11 cells with WT and glycine-to-leucine mutant hPCFTs were statistically significant (*P < 0.05). (**B**) Cells transfected with ECFP*-tagged WT and glycine-to-leucine

hPCFTs were incubated with CellMask™ Deep Red plasma membrane stain for 5 min before visualization with a Leica TCS SP5MP confocal microscope system using a 63× oil immersion lens. The excitation/emission is 649/666 nm for the plasma membrane stain and 458/460–490 nm for ECFP*.

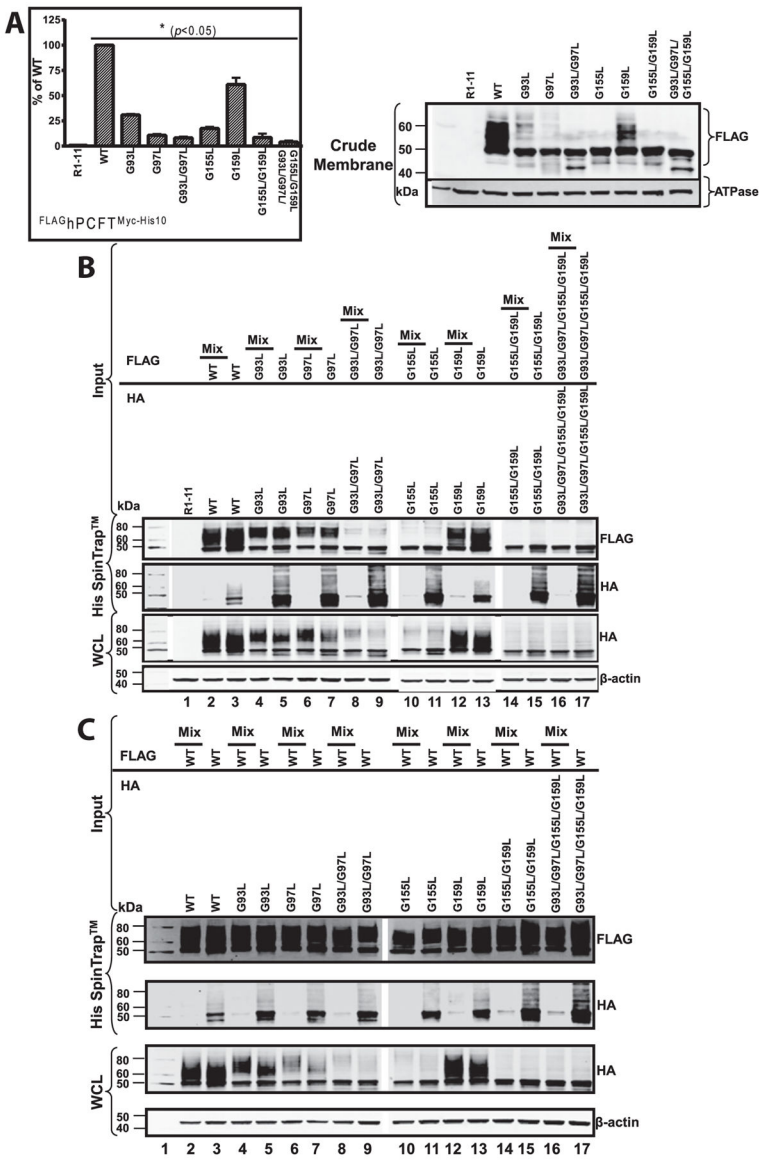

Figure 4. Co-associations of hPCFT glycine-to-leucine mutants with themselves or with WT hPCFT protein by Ni^{2+}-chelating affinity chromatography

To study the co-associations of hPCFT glycine-to-leucine mutants with themselves or with WT protein, we mutated glycine-to-leucine to obtain single (G93L, G97L, G155L, G159L) or multiple (G93L/G97L, G155L/G159L, G93L/G97L/G155L/G159L) mutants, based on *wt*^{FLAG}hPCFT$^{Myc\text{-}His10}$. (A) hPCFT WT and glycine-to-leucine ^{FLAG}hPCFT$^{Myc\text{-}His10}$ mutants were transiently transfected into hPCFT-null R1-11 cells. Transfected cells were assayed for transport at pH 5.5 with [^{3}H]Mtx (0.5 μM) for 2 min at 37°C (left panel). hPCFT protein expression was measured in crude membranes by SDS/PAGE and Western blotting with FLAG antibody (right panel). Na^+/K^+ ATPase was used as a loading control. The molecular mass markers for SDS/PAGE are noted. Transport results are expressed relative to those for WT ^{FLAG}hPCFT$^{Myc\text{-}His10}$ and are reported as mean values ± standard errors from five independent experiments. The transport differences between non-transfected and

transfected R1-11 with WT and glycine-to-leucine mutant hPCFTs were all statistically significant (*$P < 0.05$). (B and C) R1-11 cells were transfected with HA-tagged glycine-to-leucine mutant, FLAG-Myc-His_{10}-tagged mutant (B) and WT hPCFT constructs (C) together (lanes with odd numbers) or separately (lanes with even numbers). Whole-cell lysates (WCL) were analysed by Western blotting prior to (lower panel) or after fractionation on His SpinTrap™ columns (upper panel) to test for protein associations. In lanes with even numbers, aliquots from separate cell transfections were mixed and chromatographed. Columns were washed with buffer (pH = 7.4) containing 120 mM imidazole and bound proteins were eluted with 500 mM imidazole. β-Actin was used as a loading control.

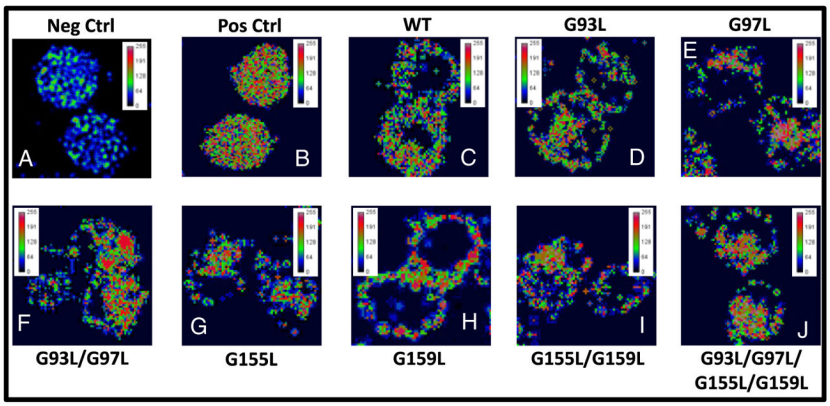

Figure 5. Co-association of hPCFT glycine-to-leucine mutant by FRET

Expression constructs for YPet plus ECFP* (negative control), YPet-ECFP* tandem (positive control), YPet–hPCFT WT plus hPCFT–ECFP* WT and YPet–hPCFT mutants plus their corresponding hPCFT–ECFP* mutant (test samples) constructs were transiently transfected into R1-11 cells. R1-11 cells were also singly transfected with YPet, ECFP*, YPet–hPCFT WT or mutant constructs and with hPCFT–ECFP* WT or mutant constructs as FRET controls (result not shown). Forty-eight hours post-transfection, YPet and ECFP* images were acquired on a Leica TCS SP5MP confocal microscope system and total donor (ECFP*), total acceptor (YPet) and sensitized FRET emissions (NET FRET) were calculated. Images collected in the FRET channel were calculated and representative images for each sample are shown. Calculated FRET values for both test samples and controls are represented using a pseudo colour scale.

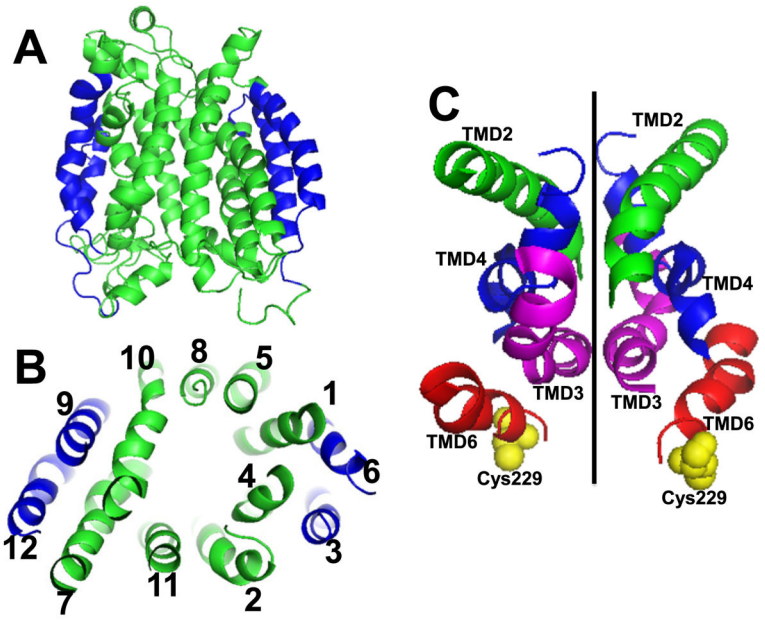

Figure 6. 3D homology models for hPCFT

(**A** and **B**) Using Robetta as a modelling platform with GlpT as template [49] and based on experimental results and bibliographic data mining, we generated a 3D homology model for monomeric hPCFT in which TMDs 1, 2, 4, 5, 7, 8, 10 and 11 comprise an aqueous transmembrane pathway, flanked by TMDs 3, 6, 9 and 12. (**C**) A molecular model is shown for dimeric hPCFT, predicted with MDOCK [51] and based on experimental data in the present study, as described in the text. The model predicts that TMDs 2, 3, 4 and 6 in hPCFT form critical structural interfaces between hPCFT monomers.

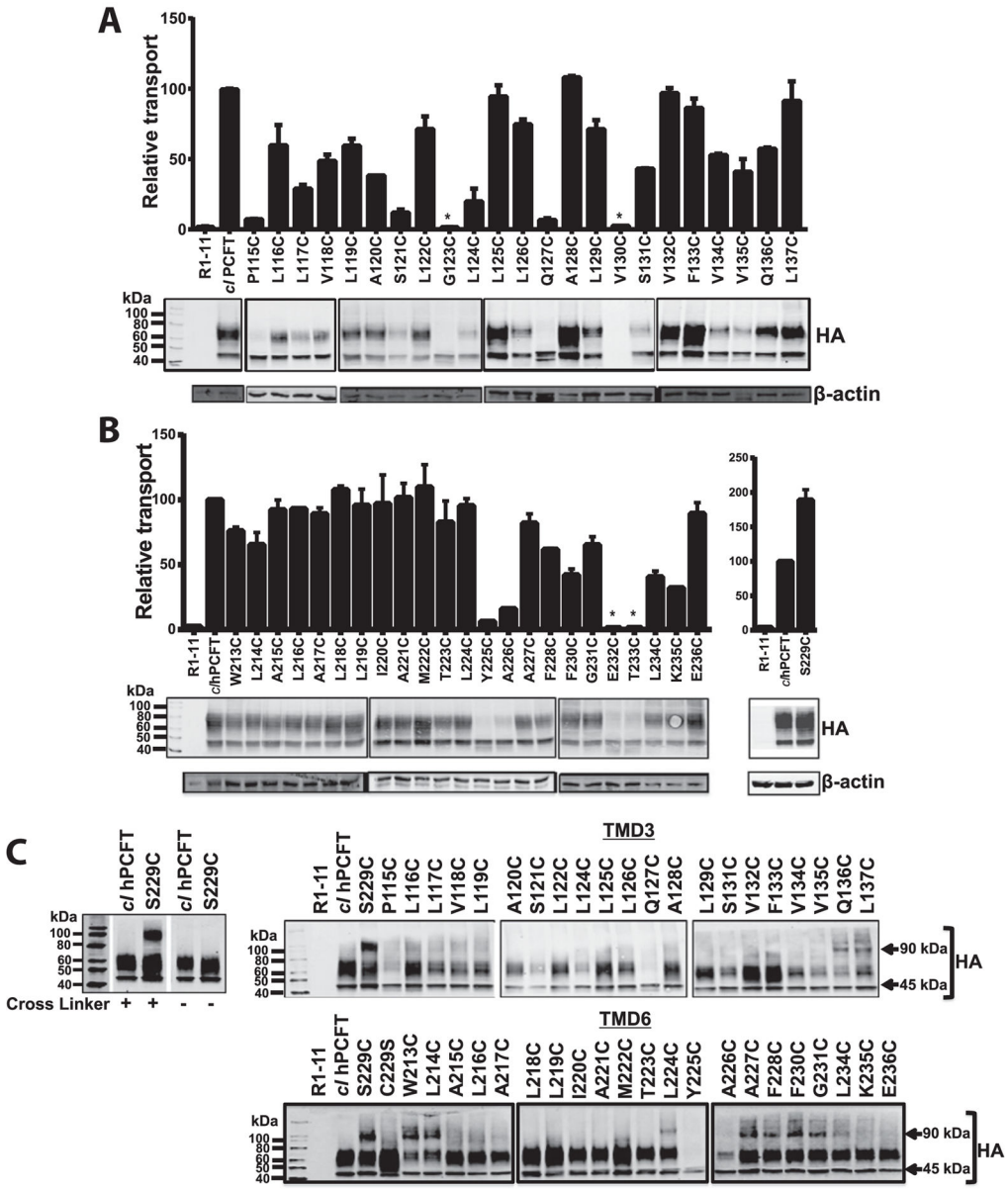

Figure 7. MTS-6-MTS cross-linking of TMD3 and TMD6 cysteine-insertion mutants in cysteine-less hPCFT^{HA}

To characterize the transport function and protein expression of single-cysteine mutants of hPCFT, single-cysteine mutants of TMD3 (**A**) and TMD6 (**B**) were transiently transfected into hPCFT-null R1-11 cells. Transfected cells were assayed for transport at pH 5.5 with [^{3}H]Mtx (0.5 μM) for 2 min at 37°C. hPCFT protein expression was measured in crude membranes by SDS/PAGE and Western blotting with HA-specific antibodies. β-Actin was used as a loading control. The molecular mass markers for SDS/PAGE are noted. Transport results are expressed relative to those for *cl*hPCFT^{HA} and are reported as mean values ± standard errors from two independent experiments. (**C**), Single cysteine mutants (HA-tagged) of TMD6 (from positions 213–236) and TMD3 (from positions 115–137) in a *cl*hPCFT^{HA} background were transiently transfected into R1-11 cells and 48 h later cells

were treated with the MTS-6-MTS cross-linker (0.3 mM for 1 h on ice). *cl*hPCFT^{HA} and S229C hPCFT^{HA} with and without cross-linker treatment were included as controls. Cells were harvested and membrane proteins were analysed on Westerns with anti-HA antibody. The hPCFT monomer migrates at ~45 kDa and cross-linked hPCFT migrates at ~90 kDa. The molecular mass markers for SDS/PAGE are noted.